Factors affecting imine coordination in (iminoterpyridine)MX$_2$ (M = Fe, Co, Ni, Zn): synthesis, structures, DFT calculations and ethylene oligomerisation studies

Yohan D. M. Champouret,[a] Jean-Didier Maréchal,†[ab] Rajinder K. Chaggar,[a] John Fawcett,[a] Kuldip Singh,[a] Feliu Maseras[c] and Gregory A. Solan*[a]

The bulky arylimino-terpyridine ligands, 6-{(2,6-i-Pr$_2$C$_6$H$_3$)N=CR}-2,2′:6′,2″-C$_{15}$H$_{10}$N$_3$ [R = H (L1), Me (L2)], have been prepared in high yield from the condensation reaction of the corresponding carbonyl compound with one equivalent of 2,6-diisopropylaniline. Interaction of an equimolar ratio of MX$_2$ with aldimine-containing L1 in n-BuOH at 110 °C affords the mononuclear five-coordinate complexes, [(L1)MX$_2$] (M = Fe, X = Cl **1a**; M = Co, X = Cl **1b**; M = Ni, X = Br **1c**; M = Zn, X = Cl **1d**), in which the metal centres occupy the terpyridine cavities in L1 with the imino group pendant and *exo* to the adjacent pyridine nitrogen atom. Similarly, a five-coordinate complex [(L2)ZnCl$_2$] (**2d**) is accessible from the reaction of ketimine-containing L2 with ZnCl$_2$ with the non-coordinated imine group in **2d**, in this case, adopting a pseudo-*exo* configuration. In contrast, coordination of the imino-nitrogen atom (*endo* configuration) results on reaction of (DME)NiBr$_2$ (DME = 1,2-dimethoxyethane) with L2 to furnish the six-coordinate complex *trans*-[(L2)NiBr$_2$] (**2c**). With [(L2)MCl$_2$] (M = Fe **2a**; M = Co **2b**) both solution and solid state IR spectroscopy suggest that the imine group prefers to adopt a bound conformation. Quantum mechanical calculations (DFT) have been performed on [(Lx)MX$_2$] (Lx = L1, L2; M = Fe, Co, Ni, Zn; X = Cl, Br) and support the synthetic results with the *exo* conformations energetically preferred for **1a–1d** and **2d**, while a distinct energetic preference is observed for the *endo* conformation in **2c**. For **2a** and **2b**, however, the closeness in energies for *endo* and *exo* configurations suggests dynamic behaviour is likely. The iron species **1a** and **2a** display low activities (on treatment with excess MAO) for ethylene oligomerisation at one bar ethylene pressure affording highly linear α-olefins (>98%); the cobalt (**1b**, **2b**) and nickel (**1c**, **2c**) species are inactive. Single crystal X-ray diffraction studies have been performed on **1a**, **1b**, **1d**, **2c** and **2d**.

1. Introduction

In spite of the rich variety of transition metal complexes of 2,2′:6′,2″:6″,2‴-quaterpyridine (A, Fig. 1) that have been reported,[1–5] the coordination chemistry of closely related 2,6-linked oligopyridylimine N,N,N,N-ligands such as 6,6′-bis(arylimino)-2,2′-bipyridine (B, Fig. 1) is not nearly as well developed. Nevertheless, the role of B in both supramolecular chemistry[6] and metal-mediated alkene polymerisation/oligomerisation catalysis[7] has been documented. On the other hand 6-arylimino-2,2′:6,2″-terpyridine (Lx, Fig. 1), a hybrid of A and B, has to the knowledge of the authors not been investigated as a support for metal complexes.

Recently, we have been interested in the coordination chemistry and catalytic potential of divalent late transition metal complexes containing the more extended oligopyridyl-imine ligand, 6,6″-bis(arylimino)-2,2′:6′,2″-terpyridine (C, Fig. 1).[8] By judicious choice of imino-carbon substituent (R) in C, 1 : 1 coordination compounds incorporating the metal centre in either a tridentate terpyridyl (R = H) or a tetradentate iminoterpyridyl (R = Me) cavity have been structurally identified for Ni(II). By contrast, attempted isolation of a 1 : 1 complex featuring Zn(II) and the ketimine derivative of C (R = Me) furnished only a dinuclear Zn$_2${bis(arylimino)-terpyridine}-containing species. This variation in bonding capacity has prompted us to target related ligand frames in which bimetallic formation is unlikely.

Herein, the use of the shorter chain mono-imine Lx (Fig. 1) is investigated as a support for a series of late transition metal(II) halides. In particular, we employ a combined synthetic and theoretical approach to study the factors that influence the capacity of 6-{(2,6-i-Pr$_2$C$_6$H$_3$)N=CR}-2,2′:6′,2″-C$_{15}$H$_{10}$N$_3$ [L1 (R = H$_{aldimine}$), L2 (R = Me$_{ketimine}$)] to act as tri- or tetra-dentate (or both) ligands in complexes

[a] Department of Chemistry, University of Leicester, University Road, Leicester, UK LE1 7RH. E-mail: gas8@leicester.ac.uk
[b] Department of Biochemistry, University of Leicester, University Road, Leicester, UK LE1 7RH
[c] Institute of Chemical Research of Catalonia (ICIQ), Av. Països Catalans, 16, 43007 Tarragona, Spain
† Present address: Institute of Biochemistry and Biophysics Molecular and Cellular Bât 430, Université Paris Sud, XI 91405 Orsay Cedex, France.
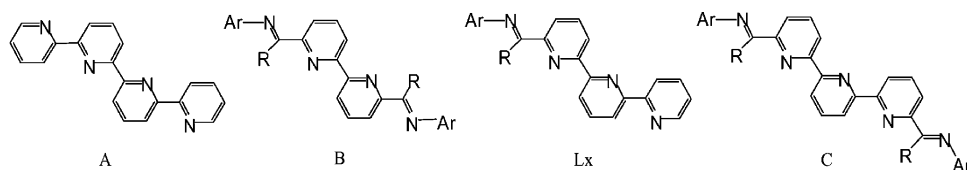
Fig. 1 Quaterpyrine (A), bis(imino)bipyridine (B), terpyridylimine (Lx) and bis(imino)terpyridine (C); R = H or methyl, Ar = aryl group.

based on the 3d metals, iron, cobalt, nickel and zinc. In addition, several of these systems are probed as precatalysts for the oligomerisation of ethylene and their performances related to the bonding modes possible for Lx.

## 2. Results and discussion

2.1. Ligand synthesis

Ligands 6-{(2,6-i-Pr$_2$C$_6$H$_3$)N=CR}-2,2′:6′,2″-C$_{15}$H$_{10}$N$_3$ [R = H (L1), Me (L2)] can be prepared by treating the corresponding carbonyl compound, 6-{O=CR}-2,2′:6′,2″-C$_{15}$H$_{10}$N$_3$ (R = H, Me), with 2,6-diisopropylaniline in absolute ethanol in the presence of a catalytic amount of glacial acetic acid. To achieve satisfactory yields, the synthesis of aldimine-containing L1 required milder conditions and shorter reaction times (50 °C, 12 hours) while for L2 higher temperatures and longer reaction times (80 °C, 72 hours) were found to be more suitable (Scheme 1). Alternatively, L2 can be prepared by reacting 6-{O=CMe}-2,2′:6′,2″-C$_{15}$H$_{10}$N$_3$ in neat 2,6-diisopropylaniline at 160 °C over a 30 minute reaction time.[9] The precursor carbonyl compounds are not commercially available and are synthesised by using either a palladium(0)-mediated cross-coupling of 6-bromo-2,2′-bipyridine[9] with 2-(n-Bu$_3$Sn)-6-{C(R)CH$_2$CH$_2$O}-C$_5$H$_3$N (R = H, Me) or by treating the lithiated derivative of 6-bromo-2,2′:6′-2″-terpyridine with Me$_2$NCRO (R = H, Me) using conditions established by Tanaka *et al.* for the formyl derivative 6-{O=CH}-2,2′:6′,2″-C$_{15}$H$_{10}$N$_3$ (Scheme 1).[10]

2.2 Synthesis of complexes

The reaction of L1 or L2 with one equivalent of MX$_2$ [MX$_2$ = FeCl$_2$, CoCl$_2$, (DME)NiBr$_2$, ZnCl$_2$] in n-butanol at 110 °C gave complexes [(L1)MX$_2$] (M = Fe, X = Cl **1a**; M = Co, X = Cl **1b**; M = Ni, X = Br **1c**; M = Zn, X = Cl **1d**) and [(L2)MX$_2$] (M = Fe, X = Cl **2a**; M = Co, X = Cl **2b**; M =

Ni, X = Br **2c**; M = Zn, X = Cl **2d**) in high yield, respectively (Scheme 2). All products have been characterised by FAB mass spectrometry, IR spectroscopy and, in the cases of **1a–c** and **2a–c** by magnetic measurements and diamagnetic **1d/2d** by ^{1}H NMR spectroscopy (see Table 1 and Experimental section). In addition, crystals of **1a**, **1b**, **1d**, **2c** and **2d** have been the subject of single crystal X-ray diffraction studies.

Crystals of **1** suitable for the X-ray determinations were grown from acetonitrile (**1a**, **1b**) or from a mixed chloroform–acetonitrile (**1d**) solution. The structures of **1a**, **1b** and **1d** belong to an isomorphous series and will be discussed together. A view of **1a** is depicted in Fig. 2; selected bond distances and angles for **1a**, **1b** and **1d** are listed in Table 2. Each structure consists of a five-coordinate metal centre surrounded by two chloride ligands and three pyridyl groups from L2 with the imino group non-coordinated. With the geometric parameter (τ) in **1a**, **1b** and **1d** being close to 0.5 > τ = 0.39 (**1a**), 0.51 (**1b**), 0.46 (**1d**)],[11] geometries based on distorted trigonal bipyramidal or distorted square pyramidal could both be applicable. Nevertheless, in **1a** and **1d** a slight
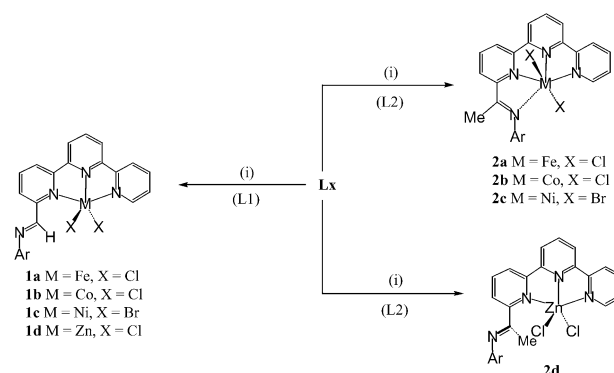
Scheme 2 *Reagents and conditions*: (i) MX$_2$ [MX$_2$ = FeCl$_2$, CoCl$_2$, ZnCl$_2$, (DME)NiBr$_2$], n-butanol, 110 °C (Ar = 2,6-i-Pr$_2$C$_6$H$_3$).
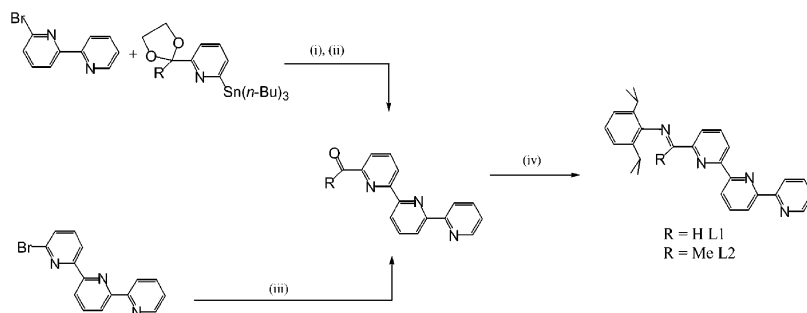
Scheme 1 *Reagents and conditions*: (i) Pd(PPh$_3$)$_4$ (6 mol%), toluene, 90 °C, 72 h; (ii) HCl (4 M), 60 °C, 12 h; (iii) n-BuLi, −78 °C, Me$_2$NC(O)R (R = H, Me), diethyl ether–hexane–tetrahydrofuran; (iv) 2,6-i-Pr$_2$C$_6$H$_3$NH$_2$, cat. H$^+$, ethanol, 50–80 °C, 12–72 h.

Table 1 Selected characterisation data for complexes **1** and **2**

Compound	Colour	$\nu(C=N)^a/$ cm^{-1}	μ_{eff}^b/μ_B	^{1}H NMR spectrum^c	FAB mass spectrum
1a	Purple-blue	1637	5.2	^{e}	546 [M]$^+$, 511 [M − Cl]$^+$
1b	Blue-green	1644	4.3	^{e}	514 [M − Cl]$^+$, 479 [M − 2Cl]$^+$
1c	Orange	1639	2.5	^{e}	559 [M − Br]$^+$, 478 [M − 2Br]$^+$
1d	Pale yellow	1644	^{d}	1.23 (d, 12H, $^3J_{HH}$ 7.0 Hz, CH(CH_3)$_2$), 3.12 (sept, 2H, $^3J_{HH}$ 7.0 Hz, CH(CH$_3$)$_2$), 7.1–7.2 (m, 3H, ArH), 7.6 (m, 1H, PyH), 8.04 (dd, 1H, $^3J_{HH}$ 7.6 Hz, $^4J_{HH}$ 1.4 Hz, PyH), 8.16 (app. t, 2H, $^3J_{HH}$ 7.6 Hz, $^3J_{HH}$ 7.6 Hz, PyH), 8.2–8.4 (m, 4H, PyH), 8.74 (d, 1H, $^3J_{HH}$ 7.3 Hz, PyH), 9.02 (d, 1H, $^3J_{HH}$ 5.0 Hz, PyH), 9.53 (s, 1H, HCN).	519 [M − Cl]$^+$, 484 [M − 2Cl]$^+$
2a	Dark purple	1594	5.3	^{e}	525 [M − Cl]$^+$, 490 [M − 2Cl]$^+$
2b	Blue	1569	4.6	^{e}	528 [M − Cl]$^+$, 493 [M − 2Cl]$^+$
2c	Orange	1575	2.6	^{e}	573 [M − Br]$^+$, 492 [M − 2Br]$^+$
2d	Pale yellow	1634	^{d}	1.07 (d, 12H, $^3J_{HH}$ 7.0 Hz, CH(CH_3)$_2$), 2.56 (s, 3H, CH_3CN), 2.93 (sept, 2H, $^3J_{HH}$ 7.0 Hz, CH(CH$_3$)$_2$), 7.4–7.5 (m, 3H, ArH), 7.6 (m, 1H, PyH), 7.8 (m, 1H, 1.4 Hz, PyH), 8.25 (ddd, 1H, $^3J_{HH}$ 7.9 Hz, $^3J_{HH}$ 7.9 Hz, $^4J_{HH}$ 1.5 Hz, PyH), 8.40 (d, 1H, $^3J_{HH}$ 7.9 Hz, PyH), 8.4–8.6 (m, 5H, PyH), 8.66 (d, 1H, $^3J_{HH}$ 7.9 Hz, PyH).	533 [M − Cl]$^+$, 498 [M − 2Cl]$^+$

^{a} Recorded on a Perkin-Elmer Spectrum One FT-IR spectrometer on solid samples. ^{b} Recorded on an Evans balance at room temperature. ^{c} Recorded in CDCl$_3$ (**1d**) and CD$_3$CN (**2d**) at ambient temperature. ^{d} Sample is diamagnetic. ^{e} Broad paramagnetically shifted peaks.

preference towards distorted square pyramidal ($\tau < 0.5$) is observed, as is the case for other experimental and calculated five-coordinate structures determined in this work (*vide infra*). The pyridyl nitrogen–metal distances are unsymmetrical with the central N(2)$_{py}$–M(1) distance being the shortest [2.1081(19) (**1a**), 2.0302(15) (**1b**), 2.0729(18) (**1d**) Å] and the distance involving the imine-substituted pyridyl [N(3)$_{py}$] group the longest [2.2214(19) (**1a**), 2.1937(16) (**1b**), 2.2574(18) (**1d**) Å]. Between structures the nitrogen–cobalt distances in **1b** are shorter than the corresponding values in **1a** and **1d**, consistent with the ionic radii for a high spin dipositive cobalt ion being smaller than for iron and zinc. The pendant imino group in each structure [C(16)–N(4) 1.263(3)–1.264(3) Å] is *exo* and almost coplanar to the adjacent coordinated pyridine groups [*tors*: N(3)–C(15)–C(16)–N(4) 174.6° (**1a**), 174.0° (**1b**), 168.2°

(**1d**)] with the *N*-aryl unit essentially orthogonal to these planes.

The preference of the MX$_2$ unit in **1** to occupy uniquely the terpyridyl cavity within L1 has also been observed in the related 1 : 1 bis(aldimino)terpyridyl [{(2,6-*i*-Pr$_2$C$_6$H$_3$N=CH)$_2$terpy}MX$_2$] (M = Fe, Ni, Zn, X = halide) complexes.[8] However when a sequence of only two pyridine units is present within the oligopyridylimine chain, imine coordination can be achieved. For example, in the bis(aldimino)bipyridyl series, [{(2,6-*i*-Pr$_2$C$_6$H$_3$N=CH)$_2$bipy}MCl$_2$] (M = Fe,[7] Ni[12]), the MX$_2$ unit fills the tridentate dipyridylimine pocket leaving the remaining aldimine unit unbound. Nevertheless, an *exo* conformation for the pendant CH=NAr unit is a feature of all the above structural types contrasting with the pseudo-*endo* disposition observed by the non-coordinated pyridine nitrogen
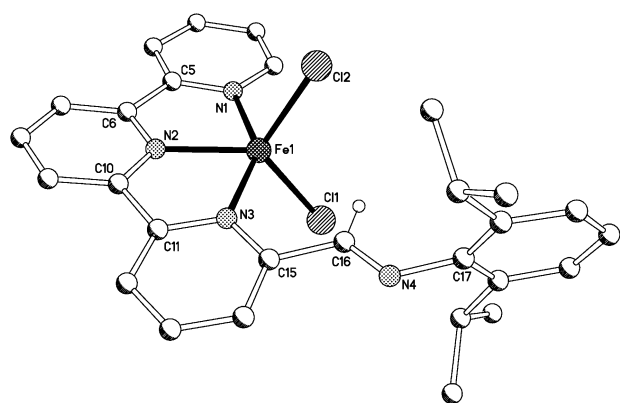

Fig. 2 Molecular structure of **1a** including the atom numbering scheme. All hydrogen atoms, apart from H16, have been omitted for clarity.

Table 2 Selected bond distances (Å) and angles (°) for **1a**, **1b** and **1d**

|	**1a** (M = Fe)	**1b** (M = Co)	**1d** (M = Zn)
M(1)–N(1)	2.175(2)	2.1514(16)	2.1935(19)
M(1)–N(2)	2.1081(19)	2.0302(15)	2.0729(18)
M(1)–N(3)	2.2214(19)	2.1937(16)	2.2574(18)
M(1)–Cl(1)	2.2868(8)	2.2630(7)	2.2429(6)
M(1)–Cl(2)	2.3081(7)	2.2733(7)	2.2548(7)
C(16)–N(4)	1.264(3)	1.263(2)	1.263(3)
N(1)–M(1)–N(2)	74.48(8)	76.64(6)	75.28(7)
N(1)–M(1)–N(3)	148.97(8)	153.29(6)	150.47(7)
N(2)–M(1)–N(3)	74.53(7)	76.71(6)	75.24(7)
Cl(1)–M(1)–Cl(2)	114.93(3)	117.76(3)	117.37(3)
Cl(1)–M(1)–N(1)	97.41(6)	95.34(5)	97.68(5)
Cl(1)–M(1)–N(2)	125.48(6)	122.84(5)	119.87(5)
Cl(1)–M(1)–N(3)	99.22(5)	97.38(4)	98.39(5)
Cl(2)–M(1)–N(1)	94.55(6)	93.95(5)	95.48(5)
Cl(2)–M(1)–N(2)	119.39(6)	119.20(5)	122.72(5)
Cl(2)–M(1)–N(3)	101.84(5)	100.68(5)	98.88(5)
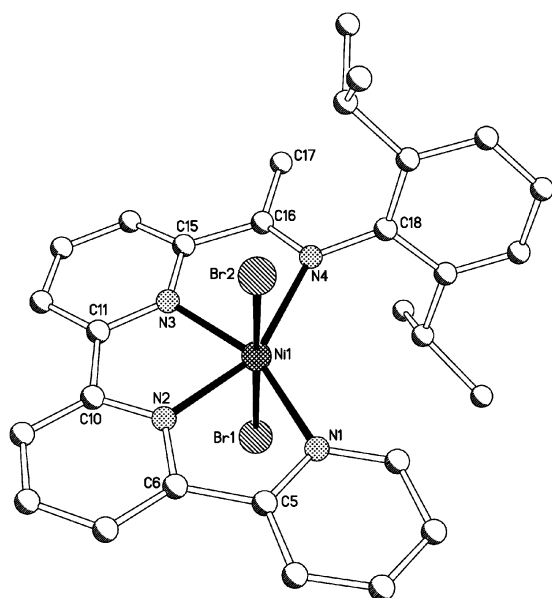
Fig. 3 Molecular structure of **2c** including the atom numbering scheme. All hydrogen atoms have been omitted for clarity.

atoms (one per quaterpyridine) in octahedral [(quaterpyridine)$_2$Fe](ClO$_4$)$_2$.[3b]

Complexes **1a–d** all show molecular ion peaks and/or fragmentation peaks corresponding to the loss of halide ions. In their infrared spectra (in solution or in solid state) ν(C=N) bands are seen at *ca.* 1640 cm^{-1} corresponding to a non-coordinated imine group and in a similar region to that for the free ligand L1.[8] Complexes **1a–c** are paramagnetic and exhibit magnetic moments of 5.2 μ_B, 4.3 μ_B and 2.5 μ_B (Evans balance at ambient temperature), values that are typical of high spin configurations corresponding to four, three, and two unpaired electrons, respectively. In the ^{1}H NMR spectrum of diamagnetic **1d**, signals characteristic for the aryl-H and pyridyl-H protons are seen along with a singlet at δ 9.53 for the aldimine C*H*=N proton which is shifted by *ca.* δ 1.2 downfield in comparison with the corresponding signal in free L1. The presence of only one doublet for the CH*Me*$_2$ protons suggests that free rotation around the aryl–nitrogen bond is operational further supporting the non-coordination of the imine.

Crystals of **2c** suitable for X-ray determination were grown by prolonged standing in chloroform. A view of **2c** is shown in
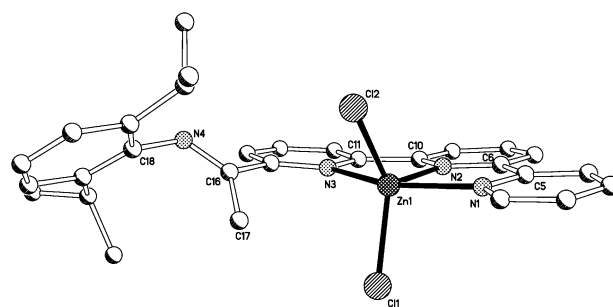
Fig. 4 Molecular structure of **2d** including the atom numbering scheme. All hydrogen atoms have been omitted for clarity.

Fig. 3; selected bond distances and angles are listed in Table 3. The molecular structure comprises a single nickel atom bound by both L2 and two terminal bromide ligands so as to form a distorted octahedral geometry. The bromide ligands are disposed mutually *trans* [Br(1)–Ni(1)–Br(2) 175.74(10)°] with all the four nitrogen donor atoms of L2 filling the equatorial belt. The pyridyl nitrogen–nickel distances are unequally disposed with the internal pyridyl distances being the shortest [Ni(1)–N(2) 1.953(12) Å, Ni(1)–N(3) 1.972(10) Å] and the external pyridyl lengths the longest [Ni(1)–N(1) 2.064(12) Å]. Of the four nitrogen donor moieties, the imino nitrogen forms the longest distance to nickel [Ni(1)–N(4) 2.191(12) Å] with its N-aryl group located almost orthogonal to the terpyridylimine plane. The tetradentate bonding mode exhibited by L2 in **2c** is in contrast to the tridentate mode adopted by L1 in **1** but resembles that found in the 1 : 1 complexes *trans*-[(quaterpyridine)Ni(L)$_2$](NCA) (L = NCMe, NCA = PF$_6$;[4d] L = OH$_2$, NCA = BF$_4$[4i]) and the ketimine-containing complex *trans*-[{(2,6-*i*-Pr$_2$C$_6$H$_3$N=CMe)$_2$terpy}NiBr$_2$].[9]

Crystals of **2d** suitable for X-ray determination were grown from a mixed chloroform–acetonitrile solution. A view of **2d** is shown in Fig. 4; selected bond distances and angles are listed in Table 4. The structure of **2d** resembles **1d** with a five-coordinate zinc centre surrounded by two chloride ligands and three pyridyl groups from L2 with the CMe=NAr group non-coordinated. The geometry at the metal centre is also distorted square pyramidal [τ = 0.35][11] with the N(2) atom defining the apical site and N(1), N(3), Cl(1) and Cl(2) the basal ones. However unlike **1d**, the non-coordinated imine group adopts a pseudo-*exo* configuration [*tors.*: N(3)–C(15)–C(16)–N(4) 146.3°] with respect to the adjacent coordinated pyridine group. The deviation from planarity is likely due to steric hindrance that can occur between the

Table 3 Selected bond distances (Å) and angles (°) for **2c**

Ni(1)–N(1)	2.064(12)	Ni(1)–Br(1)	2.579(2)
Ni(1)–N(2)	1.953(12)	Ni(1)–Br(2)	2.514(2)
Ni(1)–N(3)	1.972(10)	C(16)–N(4)	1.313(16)
Ni(1)–N(4)	2.191(12)	C(16)–C(17)	1.504(19)
N(1)–Ni(1)–N(2)	79.9(4)	N(2)–Ni(1)–Br(1)	88.5(3)
N(1)–Ni(1)–N(3)	157.0(5)	N(2)–Ni(1)–Br(2)	88.8(3)
N(1)–Ni(1)–N(4)	154.1(4)	N(3)–Ni(1)–N(4)	77.3(4)
N(2)–Ni(1)–N(3)	77.4(5)	N(3)–Ni(1)–Br(1)	86.5(3)
N(2)–Ni(1)–N(4)	154.1(4)	N(3)–Ni(1)–Br(2)	96.2(3)
Br(1)–Ni(1)–Br(2)	175.74(10)	N(4)–Ni(1)–Br(1)	95.4(3)
N(1)–Ni(1)–Br(1)	89.3(3)	N(4)–Ni(1)–Br(2)	88.4(3)
N(1)–Ni(1)–Br(2)	87.0(3)		

Table 4 Selected bond distances (Å) and angles (°) for **2d**

Zn(1)–N(1)	2.193(2)	Zn(1)–Cl(2)	2.2322(9)
Zn(1)–N(2)	2.069(2)	C(16)–N(4)	1.281(4)
Zn(1)–N(3)	2.308(2)	C(16)–C(17)	1.465(4)
Zn(1)–Cl(1)	2.2654(9)		
N(1)–Zn(1)–N(2)	75.18(9)	N(1)–Zn(1)–Cl(2)	95.59(7)
N(1)–Zn(1)–N(3)	150.70(9)	N(2)–Zn(1)–Cl(1)	110.85(7)
N(2)–Zn(1)–N(3)	75.69(9)	N(2)–Zn(1)–Cl(2)	119.32(7)
Cl(1)–Zn(1)–Cl(2)	129.60(3)	N(3)–Zn(1)–Cl(1)	100.75(6)
N(1)–Zn(1)–Cl(1)	92.49(7)	N(3)–Zn(1)–Cl(2)	95.82(6)

imino-methyl and the chloride ligands. The effect of this steric interaction appears also to impact on the N(3)–Zn(1) distance with a noticeably longer bond in **2d** when compared with **1d** [2.308(2) (**2d**) *vs.* 2.2574(18) (**1d**) Å].

In the IR spectra for **2a–d** (recorded in the solid state), ν(C=N) bands are seen between 1634–1569 cm^{-1} with the band for **2d** (1634 cm^{-1}) falling at the higher end of the range and consistent with a non-coordinated imine group. In contrast, **2c** shows no C=N stretch above 1575 cm^{-1} while in **2a** and **2b** only very weak bands at *ca.* 1630 cm^{-1} are apparent suggesting that the bound imine is the preferred configuration. The FAB mass spectra of **2a–2d** each show fragmentation peaks corresponding to the loss of one and two halide ions. The high spin nature of **2a–c** is confirmed from magnetic measurements which indicate moments of 5.3 μ_B, 4.6 μ_B and 2.6 μ_B (Evans balance at ambient temperature), their magnitude being consistent with the presence of four, three, and two unpaired electrons, respectively.

In the ^1H NMR spectrum of diamagnetic **2d**, sharp signals are seen for the aryl-H and pyridyl-H protons along with a singlet at δ 2.56 corresponding to the C*Me*=N group; shifted by *ca.* 0.3 ppm downfield in comparison with free L2. The isopropyl methyl protons are seen as a single doublet at δ 1.07 suggesting that as with **1d** the *N*-aryl group in **2d** can freely rotate, indicating that the imine is not bound. By contrast the ^1H NMR spectrum of **2c** shows broad paramagnetically shifted peaks between δ −4.1 and 130.9 (see Experimental section). Some degree of assignment can be made on comparison of the chemical shifts and relaxation times with previously reported nickel(II)–pyridyl systems.[13] For example, the single pyridyl-H$_\alpha$ proton can be identified as the most downfield signal (δ 130.9), the six pyridyl-H$_\beta$ and pyridyl-H$_{\beta'}$ protons to the signals at δ 92.9, 82.5, 72.3, 66.8, 59.5, 35.0 while the pyridyl-H$_\gamma$ protons are assigned to the more upfield signals at δ 18.0, 16.9, 13.3. A related assignment of the signals for **2a**

and **2b**, however, proved problematic due to the poor solubility of the complexes and extreme broadness of the signals. Nevertheless, the pyridyl-H$_\alpha$ protons could be identified as peaks at δ 103.4 and δ 95.2 for **2a** and **2b**, respectively.

2.3 Density functional theory calculations

Given our recent findings on the flexibility of coordination behaviour exhibited by the more extended oligopyridylimine C (see Fig. 1),[8] the capacity of L*x* to adopt both tri- (with imino group *exo*) or tetra-dentate (with imino group *endo*) bonding modes on coordination to an M*X*$_2$ unit was not entirely surprising. In this previous study the nature of the imino-carbon substituent (Me *vs.* H) was found to be highly influential on the bonding mode displayed by the ligand while the role of the 3d metal centre (or possibly the halide employed) was not clear. To complement the synthetic work undertaken herein and to compare with our previous studies, DFT calculations have been performed on [(L*x*)MX$_2$] (M = Fe, Co, Ni, Zn; X = Cl, Br) for both L1 and L2 with the intent of understanding more fully the factors that influence the binding mode of L*x*.

In order to evaluate the validity of our DFT approach, geometry optimisations have initially been performed on selected complexes that have been the subject of X-ray determinations in this work. Specifically, optimised structures of *trans*-[(L2)NiBr$_2$] (*opt*-**2c**$_{endo}$), [(L1)ZnCl$_2$] (*opt*-**1d**$_{exo}$) and [(L2)ZnCl$_2$] (*opt*-**2d**$_{exo}$) were compared with the X-ray data for **2c**, **1d** and **2d**, respectively. The calculated structures are in good agreement with their respective crystallographic counterparts with their overall structural features well reproduced: octahedral for *opt*-**2c**$_{endo}$, distorted square pyramidal for *opt*-**1d**$_{exo}$ and distorted square pyramidal for *opt*-**2d**$_{exo}$ (Table 5).

With regard to *opt*-**2d**$_{exo}$, the structural arrangement of the aryl and imine moieties is maintained when compared to **2d**, though more displaced towards idealised square pyramidal

Table 5 Selected calculated bond distances (Å) and angles (°) and other structural parameters for [(L1)MX$_2$] (*opt*-**1**) and [(L2)MX$_2$] (*opt*-**2**) in both *exo*- and *endo*-conformations

	M = Fe, X = Cl				M = Co, X = Cl				M = Ni, X = Br				M = Zn, X = Cl				M = Ni, X = Cl			
	1a$_{exo}$	**2a**$_{exo}$	**1a**$_{endo}$	**2a**$_{endo}$	**1b**$_{exo}$	**2b**$_{exo}$	**1b**$_{endo}$	**2b**$_{endo}$	**1c**$_{exo}$	**2c**$_{exo}$	**1c**$_{endo}$	**2c**$_{endo}$	**1d**$_{exo}$	**2d**$_{exo}$	**1d**$_{endo}$	**2d**$_{endo}$	**1c'**$_{exo}$	**2c'**$_{exo}$	**1c'**$_{endo}$	**2c'**$_{endo}$
Bond lengths																				
M(1)–N(1)	2.25	2.25	2.23	2.22	2.19	2.2	2.15	2.17	2.13	2.13	2.12	2.11	2.25	2.27	2.32	2.31	2.13	2.13	2.13	2.13
M(1)–N(2)	2.13	2.12	2.19	2.2	2.1	2.07	2.14	2.12	2.02	1.99	2.04	2.03	2.19	2.16	2.23	2.22	2.02	1.99	2.04	2.04
M(1)–N(3)	2.28	2.35	2.18	2.18	2.2	2.26	2.12	2.1	2.16	2.17	2.03	2.02	2.29	2.41	2.23	2.21	2.15	2.16	2.04	2.03
M(1)–N(4)	4.66	4.95	2.29	2.32	4.63	4.89	2.24	2.26	4.65	4.87	2.29	2.25	4.65	4.99	2.55	2.47	4.63	4.85	2.29	2.24
M(1)–X(1)	2.32	2.34	2.46	2.47	2.33	2.35	2.48	2.46	2.48	2.51	2.6	2.63	2.32	2.31	2.38	2.42	2.34	2.38	2.45	2.48
M(1)–X(2)	2.34	2.36	2.54	2.51	2.33	2.36	2.53	2.51	2.47	2.5	2.64	2.65	2.32	2.33	2.4	2.4	2.35	2.38	2.48	2.48
C(16)–N(4)	1.29	1.29	1.29	1.29	1.28	1.29	1.29	1.29	1.29	1.29	1.29	1.29	1.28	1.29	1.29	1.29	1.28	1.29	1.29	1.29
Bond angles																				
N(1)–M(1)–N(2)	75.3	75.5	74.4	73.8	75.5	76.0	75.8	76.3	78.6	79.2	78.5	78.8	73.4	73.5	72.0	72.5	78.6	79.2	78.5	78.6
N(1)–M(1)–N(3)	150.6	151.6	146.8	146.7	152.7	153.4	146.8	152.3	157.3	159.7	156.4	157.4	146.9	146.8	144.6	146.0	157.3	159.8	156.4	157.0
N(2)–M(1)–N(3)	75.4	76.6	72.4	73.3	77.2	78.4	73.9	76.1	78.7	80.5	78.0	78.6	73.7	74.5	72.6	73.5	78.7	80.6	77.9	78.4
X(1)–M(1)–X(2)	135.9	146.2	173.5	171.1	129.0	143.5	174.8	171.4	147.0	161.1	174.8	168.8	127.6	133.9	162.6	168.6	145.3	161.0	175.6	171.3
X(1)–M(1)–N(1)	94.6	91.9	85.4	85.2	91.5	89.2	86.1	89.7	91.7	89.4	88.9	87.8	96.0	94.1	85.2	85.2	92.1	89.4	87.9	89.0
X(1)–M(1)–N(2)	116.2	114.6	95.0	89.8	119.7	115.2	92.3	86.8	110.7	100.4	84.9	89.7	120.0	123.8	101.5	101.5	113.3	99.7	90.3	85.6
X(1)–M(1)–N(3)	97.5	95.1	98.1	99.4	100.4	97.5	95.6	90.9	96.0	94.1	89.4	92.6	97.9	96.3	102.2	102.2	96.2	93.9	92.3	89.2
X(2)–M(1)–N(1)	94.1	90.5	88.7	86.4	91.1	87.7	89.1	86.8	92.8	88.8	88.8	89.9	95.7	91.5	88.7	88.7	93.0	89.5	89.9	88.9
X(2)–M(1)–N(2)	107.8	98.6	86.0	85.0	110.2	99.3	84.7	84.8	102.2	97.8	83.8	85.2	112.3	105.5	92.0	92.0	101.3	98.7	85.5	85.5
X(2)–M(1)–N(3)	95.6	98.56	88.2	86.0	100.0	101.1	87.5	88.5	92.2	93.7	88.5	87.6	99.2	103.2	92.3	92.3	92.2	93.7	88.1	89.2
τ^α	0.25	0.09	—	—	0.40	0.17	—	—	0.17	0.03	—	—	0.32	0.22	—	—	0.20	0.02	—	—

^{a} τ = structural index parameter = $(\beta - \alpha)/60$ where β = the largest L–M–L angles and α = second largest (see ref. 11).

[τ = 0.35 (**2d**) *vs.* 0.22 (*opt*-**2d**$_{exo}$)]. This discrepancy is likely due to the gas phase conditions employed for the calculations which are exempt of crystal packing interactions that are evident in **2d**. While agreement between experimental and theoretical angles for *opt*-**1d**$_{exo}$, *opt*-**2c**$_{endo}$ and *opt*-**2d**$_{exo}$ are good with discrepancies less than 6°, bond lengths are slightly more divergent with average differences around 0.1 Å (Table 5). Nevertheless, the expected variations in the metal ligand distances (*e.g.*, M–N distances: Fe$_{high\ spin}$ ≈ Zn > Co$_{high\ spin}$ > Ni) between the different 3d metal complexes employed for all experimentally characterised structures are particularly well reproduced in these theoretical calculations. Due to the size of the system, it was viewed that our approach leads to good agreement with the experimental data and demonstrates that using the B3LYP functional with this basis set constitutes a viable method for studying systems described in this work. To extend the investigation, we have applied this theoretical approach to the two other X-ray characterised complexes **1a** and **1b** along with **1c**, **2a**, **2b** and the chloride analogues of **1c** and **2c**, [(L*x*)NiCl$_2$] [L*x* = L1 (**1c′**), L2 (**2c′**)].

Optimised structures for **1a**, **1b**, **1c**, **1d**, **1c′**, **2a**, **2b**, **2c**, **2d** and **2c′** have been determined based on the imine nitrogen atom being bound (*opt*-**1a**$_{endo}$, *opt*-**1b**$_{endo}$, *opt*-**1c**$_{endo}$, *opt*-**1d**$_{endo}$, *opt*-**1c′**$_{endo}$, *opt*-**2a**$_{endo}$, *opt*-**2b**$_{endo}$, *opt*-**2c**$_{endo}$, *opt*-**2d**$_{endo}$, *opt*-**2c′**$_{endo}$) and unbound (*opt*-**1a**$_{exo}$, *opt*-**1b**$_{exo}$, *opt*-**1c**$_{exo}$, *opt*-**1d**$_{exo}$, *opt*-**1c′**$_{exo}$, *opt*-**2a**$_{exo}$, *opt*-**2b**$_{exo}$, *opt*-**2c**$_{exo}$, *opt*-**2d**$_{exo}$, *opt*-**2c′**$_{exo}$); selected bond lengths and angles are listed in Table 5. By inspection of the computed structures it is evident that the *endo* conformations adopt a common octahedral structure, *trans*-[(L*x*)MX$_2$], regardless of L*x*, metal or halide (Fig. 5a). In contrast, the *exo* conformations fall into three distinct struc-

Table 6 Potential (ΔE) energies (kcal mol^{-1}) between *endo* and *exo* conformations for *opt*-**1** and *opt*-**2** using $\Delta E = E_{endo} - E_{exo}$

	ΔE		ΔE
opt-**1a**	6.7	*opt*-**2a**	0.2
opt-**1b**	9.7	*opt*-**2b**	−0.5
opt-**1c**	2.1	*opt*-**2c**	−2.5
opt-**1d**	7.5	*opt*-**2d**	3.3
opt-**1c′**	1.6	*opt*-**2c′**	−3.1

tural types: (i) with the imine co-planar to the adjacent pyridine and the metal centre adopting a distorted square pyramidal geometry (range for τ: 0.17–0.40) (Fig. 5b), (ii) with the imine unit out-of-the plane formed by the adjacent pyridine and the metal centre exhibiting a distorted square based pyramidal geometry (range for τ: 0.09–0.22) (Fig. 5c), (iii) with the imine co-planar to the adjacent pyridine, the halides disposed in a linear fashion and the metal centre displaying a more idealised square pyramidal geometry (τ = 0.02–0.03) (Fig. 5d). The particular type of *exo* conformation exhibited by a complex (Fig. 5b–d) is found to depend not only on L*x* but also on the metal centre. The nature of the halide (Cl *vs.* Br) ligand appears not to be influential in these systems. For all the L1-containing complexes (*opt*-**1**$_{exo}$), the structures adopted are based on the conformation shown in Fig. 5b with the two nickel versions displaying the more idealised square pyramidal geometries [τ = 0.17 (*opt*-**1c**$_{exo}$), 0.20 (*opt*-**1c′**$_{exo}$)]. On the other hand, complexes bound by the ketimine ligand L2 can adopt two of the *exo* structures, the precise type being determined by the metal centre with the iron, cobalt and zinc complexes (*opt*-**2a**$_{exo}$, *opt*-**2b**$_{exo}$, *opt*-**2d**$_{exo}$) preferring the
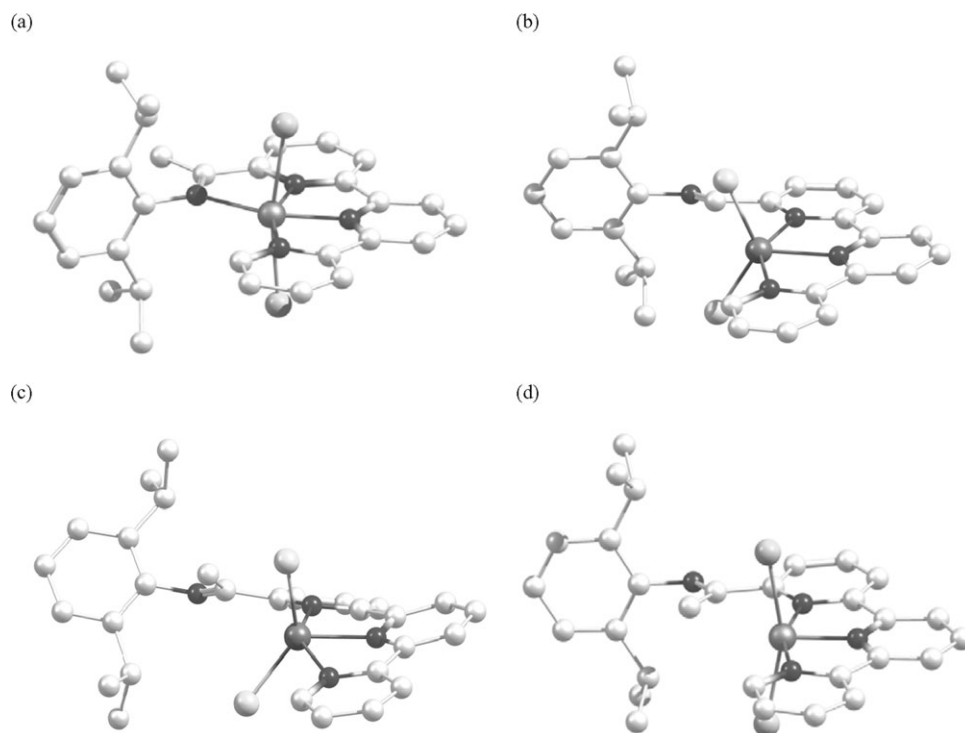

Fig. 5 Common optimised structural types for **1** and **2**: (a) *opt*-**2**$_{endo}$ (also applicable to *opt*-**1**$_{endo}$) (FeCl$_2$, CoCl$_2$, NiBr$_2$, NiCl$_2$, ZnCl$_2$); (b) *opt*-**1**$_{exo}$ (FeCl$_2$, CoCl$_2$, NiBr$_2$, NiCl$_2$, ZnCl$_2$); (c) *opt*-**2**$_{exo}$ (FeCl$_2$, CoCl$_2$, ZnCl$_2$); (d) *opt*-**2**$_{exo}$ (NiBr$_2$, NiCl$_2$).

This journal is © the Royal Society of Chemistry and the Centre National de la Recherche Scientifique 2007

structure in Fig. 5c while the nickel systems (opt-$2c_{exo}$, opt-$2c'_{exo}$) prefer that in Fig. 5d.

To investigate the relative stability of *endo versus exo* structural types for a particular L*x*–metal ion combination and to probe the potential for conformation conversions, the difference in energy between *endo* and *exo* structures for [(L1)MX$_2$] (**1**) and [(L2)MX$_2$] (**2**) was determined (Table 6).

The agreement between computed energy differences and the available experimental data is satisfactory. For species *opt-***1a**, *opt-***1b**, *opt-***1c**, *opt-***1d** and *opt-***2d**, the experimentally observed *exo*-form is favoured by a value between 2.1 and 9.7 kcal mol^{-1}. For *opt-***2c**, the experimentally observed *endo* form is computed to be more stable by 2.5 kcal mol^{-1}. Interestingly, for *opt-***2a** and *opt-***2b**, where experimental data supports the presence of the *endo* form, a small energy difference of 0.5 kcal mol^{-1} at most between the computed structures would suggest the coexistence between two species in equilibrium. Furthermore the fact that the calculations allow the least stable isomers to be computed, additional useful information can be gleaned. As highlighted above the calculations show that the behaviour depends little on the nature of the halide (Cl or Br). With regard to energy differences two major trends are apparent. The first trend is that the L1-containing systems (*opt-***1**) always favour the *exo* form with respect to the corresponding L2-containing systems (*opt-***2**), with the difference in preference oscillating between 4 and 10 kcal mol^{-1}. The second trend is that the nickel complexes (*opt-***1c**, *opt-***1c'**, *opt-***2c**, *opt-***2c'**) have a larger preference towards the *endo* form than the rest of the species, which can be quantified at ≥ 5 kcal mol^{-1}. It is also worth mentioning that both trends are additive. For example, *opt-***2c** and *opt-***2c'** are the only cases where the *endo* form is clearly favoured because of the joint presence of the ketimine L2 ligand frame and the nickel metal centre.

These trends identified in the calculations can be qualitatively rationalised. With regard to the role played by the ligands themselves, both steric and electronic effects are likely operational. The reduced donor capability of an aldimine (L1) nitrogen over a ketimine (L2) nitrogen supports the preference of L1 to adopt the *exo* form while the improved donor capacity of L2 allows *endo* configurations to be accessed.[14] In terms of steric variations, the smaller steric hindrance in L1 imparted by the H imino-carbon substituent when occupying the position closer to the metal means *exo* configurations are preferential, while for L2 the bulkier methyl substituent is less likely to adopt the *exo* configuration with the result that the *endo* arrangement will prevail. With respect to the metal centre and the resultant coordination geometries displayed, a con-

sideration of the d^n configuration is useful. For the complexes displaying five-coordinate geometries only in the case of the nickel(II) species are they adequately described as square pyramidal, while the zinc(II) species along with the high spin iron(II) and cobalt(II) systems as described as distorted square pyramidal.[15] This deviation of nickel (d^8) can be rationalised by consideration of the energy gain that would occur when the three non-bonding d-orbitals are fully occupied in the square pyramidal case (*opt-***1c**$_{exo}$, *opt-***1c'**$_{exo}$, *opt-***2c**$_{exo}$, *opt-***2c'**$_{exo}$). For Fe (d^6), Co (d^7) and Zn (d^{10}) the nature of the d^n configurations has no significant impact on the resting distorted square pyramidal geometry. Moreover, it appears that the stability of a high spin d^8-square pyramidal geometry relative to the high spin d^8-octahedral geometry is delicately balanced with the presence of the ketimine moiety in **2c** being sufficient to drive the *endo* formation. A similar but less dramatic effect is also apparent with the iron and cobalt derivatives. In the case of the zinc complexes, *endo* configurations do not form which is likely due to electron–electron repulsions between the fully occupied d-shell and the incoming imine-nitrogen donor.

2.4 Screening of complexes as catalysts for ethylene oligomerisation/polymerisation

Late transition metal complexes of the first row (*e.g.*, Fe, Co, Ni) have, in recent years, been widely employed as catalysts for alkene polymerisation and/or oligomerisation.[16] In particular, complexes containing multidentate nitrogen donor ligands incorporating bulky aryliminepyridine moieties have been central to many of the key developments, one such example being the [{(2,6-isopropylphenylimino)bipyridine)}FeCl$_2$]/ MAO system reported by Gibson *et al.* that has been shown to be highly active for alkene oligomerisation.[7] With the intent of probing the effect of an additional pyridine group within the ligand frame in the latter system, we have screened the two iron complexes (**1a** and **2a**), along with the cobalt (**1b**, **2b**) and nickel (**1d**, **2d**) species, as precatalysts for the oligomerisation/ polymerisation of ethylene.

On activation with 400 equivalents of methylaluminoxane (MAO) only the iron complexes **1a** and **2a** showed any activity for ethylene oligomerisation; the cobalt and nickel systems were inactive. The results for **1a** and **2a** employing one atmosphere of ethylene are summarised in Table 7.

Several points emerge from inspection of the data. Both complexes show only low activity for ethylene oligomerisation with the ketimine species (**2a**) showing slightly higher activity when compared with the aldimine species (**1a**). The oligomeric products are typical of iron-based catalysts giving greater than

Table 7 Ethylene oligomerisation with the iron(II) catalysts^a

Entry	Pre-catalyst	Mass^b/g	Activity/g mmol^{-1} h^{-1} bar^{-1}	Internal olefin^c (%)	External olefin^c (%)	Av. chain length,^{c} C$_n$	α^d
1	**1a**	0.040	4	1	99	16.4	0.84
2	**2a**	0.100	10	2	98	16.2	0.72

^{a} General conditions: 1 bar ethylene Schlenk test carried out in toluene (40 cm^3) at ambient temperature using 4.0 mmol MAO (Al : M = 400 : 1), 0.01 mmol precatalyst, over one hour. Reactions were terminated by addition of dilute HCl. ^{b} Mass of oligomer isolated. ^{c} Oligomerisation product percentages and average chain length, C$_n$, calculated *via* integration of ^{1}H NMR spectra. ^{d} Determined by GC; α = (rate of propagation)/ ((rate of propagation) + (rate of chain transfer)) = (moles of C$_{n+2}$)/(moles of C$_n$).

98% linear α-olefins (C6–C26). Schulz–Flory distribution of oligomers are observed in both cases with values *ca.* 0.76.[17]

The explanation for the low activity of these iron systems (**1a**/MAO or **2a**/MAO) when compared to the highly active [{(2,6-diisopropylphenylimino)bipyridine)}FeCl$_2$]/MAO[7] is uncertain but could be attributable to two reasons or a combination of both. Firstly, the imino arm **1a**/**2a** could be coordinated in the putative cationic active catalyst and thus block the approach of an incoming ethylene monomer. Indeed, this explanation has been suggested as one possible reason for the inactivity of [{bis(2,6-diisopropylphenylimino)-bipyridine}FeCl$_2$]/MAO towards ethylene.[7] Alternatively if the imino group does not coordinate, the low activity could be due to the ligand support acting more like a substituted terpyridine ligand in a manner similar to that seen in the sterically encumbered [(6,6″-diarylterpyridine)FeCl$_2$]/MAO systems in which only very low activities are reported; the steric bulk of the 6-position in this case inhibiting monomer approach.[18] Nevertheless, it is likely that the nature of the imino carbon substituent plays a key role in dictating which pathway results in a manner akin to that seen for the pre-catalytic species **1** and **2**.

3 Experimental

3.1 General

All reactions, unless otherwise stated, were carried out under an atmosphere of dry, oxygen-free nitrogen, using standard Schlenk techniques or in a nitrogen purged glove box. Solvents were distilled under nitrogen from appropriate drying agents and degassed prior to use.[19] The infrared spectra were recorded on a Perkin-Elmer Spectrum One FT-IR spectrometer on solid samples. The ES (electrospray) and the FAB mass spectra were recorded using a micromass Quattra LC mass spectrometer and a Kratos Concept spectrometer with metha-nol or NBA as the matrix, respectively. ^{1}H and ^{13}C NMR spectra were recorded on a Bruker ARX spectrometer (250 or 300 MHz) at ambient temperature; chemical shifts (ppm) are referred to the residual protic solvent peaks and coupling constants measured in Hertz (Hz). Oligomer products were analysed by GC, using a Perkin-Elmer Autosystem XL chromatograph equipped with a flame ionisation detector and 30 m PE-5 column (0.25 mm thickness), injector temperature 45 °C and the following temperature programme: 45 °C/7 min, 45–195 °C/10 °C min^{-1}, 195 °C/5 min, 195–225 °C/10 °C min^{-1}, 225 °C/5 min, 225–250 °C/10 °C min^{-1}, 250 °C/22 min. Magnetic susceptibility studies were performed using an Evans balance (Johnson Matthey) at room temperature. The magnetic moment was calculated following standard methods[20] and corrections for underlying diamagnetism were applied to the data.[21] Elemental analyses were performed at the Science Technical Support Unit, London Metropolitan University.

The reagents, 2,6-diisopropylaniline, MAO (10 wt% in toluene), metal dichlorides and (DME)NiBr$_2$ (DME = 1,2-dimethoxyethane) were purchased from Aldrich Chemical Co. and used without further purification. The compounds, 6-{(2,6-*i*-Pr$_2$C$_6$H$_3$)N═CH}$_2$–2,2′:6′,2″-C$_{15}$H$_{10}$N$_3$ (L1)[9] and 6-bromo-2,2′:6′,2″-terpyridine[22] were prepared according to

previously reported procedures. All other chemicals were obtained commercially and used without further purification.

3.2 Synthesis of 6-{(2,6-*i*-Pr$_2$C$_6$H$_3$)N═CMe}-2,2′:6′,2″-C$_{15}$H$_{10}$N$_3$ (L2)

Prepared *via* a two-step procedure:

(a) **6-Acetyl-2,2′:6,2″-terpyridine.** An oven-dried Schlenk flask equipped with a magnetic stir bar was evacuated and backfilled with nitrogen. The flask was charged with 6-bromo-2,2′:6′,2″-terpyridine (0.714 g, 2.29 mmol) and a mixture of diethyl ether (22 ml), hexane (11 ml) and tetrahydrofuran (11 ml). The solution was cooled to −78 °C and *n*-butyllithium (1.5 ml, 2.40 mmol, 1.6 M in hexane) added dropwise over 10 min resulting in a dark turquoise coloured solution. After 15 min of stirring, *N,N*-dimethylacetamide (0.43 ml, 4.58 mmol) was added and the reaction mixture stirred for a further 15 min at −78 °C. The solution was allowed to warm to room temperature and quenched with water and then left to stir overnight. The resulting deep red solution was extracted with ethyl acetate (3 × 25 ml) and the organic layer washed with saturated sodium chloride solution (3 × 25 ml) before being dried over magnesium sulfate. Following filtration the solvent was removed under reduced pressure to give a dark brown oil that solidified on prolonged standing giving a pale yellow solid. The product was crystallised from ethanol at −30 °C and collected by filtration to afford 6-acetyl-2,2′:6,2″-terpyr-idine as a pale yellow solid. Yield 80% (0.504 g, 1.83 mmol); mp: 185–187 °C. ^{1}H NMR (250 MHz, CDCl$_3$): δ 8.76 (dd, $^3J_{\text{H–H}}$ 7.7, $^4J_{\text{H–H}}$ 2.5, 1H, Py-H), 8.64 (d, $^3J_{\text{H–H}}$ 7.5, Py-H), 8.56 (d, $^3J_{\text{H–H}}$ 7.4, Py-H), 8.51 (dd, $^3J_{\text{H–H}}$ 7.5, $^4J_{\text{H–H}}$ 2,6, 1H, Py-H), 8.38 (dd, $^3J_{\text{H–H}}$ 8.0, $^4J_{\text{H–H}}$ 2.8, 1H, Py-H), 7.98 (m, 1H, Py-H), 7.87 (m, 1H, Py-H), 7.78 (m, 1H, Py-H), 7.27 (m, 1H, Py-H), 2.79 (s, 3H, C*H$_3$*C═O). ^{13}C {^{1}H} NMR (62.5 MHz, CDCl$_3$): δ 24.8 (*CH$_3$*C═O), 120.0 (Py), 120.1 (Py), 120.4 (Py), 120.5 (Py), 122.8 (Py), 122.9 (Py), 135.9 (Py), 136.7 (Py), 137.0 (Py), 148.2 (Py), 151.9 (Py), 153.5 (Py), 154.4 (Py), 154.5 (Py), 155.9 (Py), 199.4 (*C*═O). IR (cm^{-1}) 1700 (C = O), 1564, 1426, 1078, 790, 748, 668. ESIMS: *m/z* 276 [M + H]$^+$. HRMS (FAB): Calcd for C$_{17}$H$_{14}$N$_3$O [M + H]$^+$ 276.113 69, found 276.113 64.

(b) **L2.** 6-Acetyl-2,2′:6,2″-terpyridine (0.100 g, 3.64 mmol) was dissolved in the minimum quantity of absolute ethanol (10 ml) and 2,6-diisopropylaniline (0.69 ml, 3.64 mmol) along with one drop of acetic acid was introduced. The solution was heated to reflux and stirred for 72 h. On cooling to room temperature the precipitate was filtered off and washed with ethanol to give L2 as a pale yellow solid. Yield 60% (0.948 g, 2.18 mmol); mp: 242–245 °C. ^{1}H NMR (300 MHz, CDCl$_3$): δ 1.10 (d, $^3J_{\text{H–H}}$ 6.7, 12H, CH(*Me*)$_2$), 2.28 (s, 3H, CH$_3$C═N), 2.81 (sept, 2H, C*H*(Me)$_2$), 7.0–7.2 (m, 3H, Ar–H), 7.2–7.3 (m, 1H, Py-H), 7.7–7.9 (m, 1H, Py-H), 7.91 (dd, $^3J_{\text{H–H}}$ 7.9, $^3J_{\text{H–H}}$ 7.9, 2H, Py-H), 8.35 (d, $^3J_{\text{H–H}}$ 7.9, 1H, Py-H), 8.42 (d, $^3J_{\text{H–H}}$ 7.9, 1H, Py-H), 8.53 (d, $^3J_{\text{H–H}}$ 7.9, 1H, Py-H), 8.59 (d, $^3J_{\text{H–H}}$ 7.9, 1H, Py-H), 8.67 (m, 2H, Py-H). ^{13}C {^{1}H} NMR (75 MHz, CDCl$_3$): δ 16.3 (*CH$_3$*C═N), 21.9 (CH$_3$), 22.2 (CH$_3$), 27.3 (CH), 120.1 (Py), 120.2 (Py), 121.0 (Py), 122.5 (Ar), 122.8 (Ar), 134.8 (Py), 136.3 (Py), 136.8 (Py), 142.0 (Ar), 148.1 (Py),

154.4 (Py), 154.5 (Py), 155.1 (Py), 155.9 (Py), 166.1 (C=N). IR (cm^{-1}) 2952, 1630 (C=N), 1562, 1422, 1360, 1263, 1075, 990, 777, 744. ESIMS: m/z 435 [M + H]$^+$. HRMS (FAB): Calcd for $C_{29}H_{31}N_4$ [M + H]$^+$ 435.254 90, found 435.254 87.

3.3 Synthesis of [{6-iminoformyl-2,2′:6′,2″-terpyridine-(2,6-diisopropylanil)}MX$_2$] (1)

(a) 1a, M = Fe, X = Cl. An oven-dried Schlenk flask equipped with a magnetic stir bar was evacuated and back-filled with nitrogen. The flask was charged with anhydrous FeCl$_2$ (0.030 g, 0.238 mmol) in n-BuOH (10 ml) and the contents stirred at 110 °C until the iron salt had completely dissolved. L1 (0.100 g, 0.238 mmol, 1 eq.) was added and the reaction mixture stirred at 110 °C for a further 20 min. After cooling to room temperature, the suspension was concentrated and hexane added to induce precipitation of the product. The solid was filtered off, washed with hexane and dried overnight under reduced pressure to afford [{6-{(2,6-i-Pr$_2$C$_6$H$_3$)N=CH}-2,2′:6′,2″-C$_{15}$H$_9$N$_3$}FeCl$_2$] (1a) as a purple-blue powder. Yield: 68% (0.088 g, 0.162 mmol). Recrystallisation from a hot acetonitrile solution gave 1a as purple plates. Anal. Calcd for $C_{28}H_{28}N_4FeCl_2$: C, 61.43; H, 5.12; N, 10.24. Found C, 60.69; H, 5.06; N, 10.30%.

(b) 1b, M = Co, X = Cl. Using an analogous procedure to that described for 1a employing CoCl$_2$ (0.031 g, 0.238 mmol) and L1 (0.100 g, 0.238 mmol, 1 eq.) gave [{6-{(2,6-i-Pr$_2$C$_6$H$_3$)N=CH}-2,2′:6′,2″-C$_{15}$H$_9$N$_3$}CoCl$_2$] (1b) as a blue-green powder. Yield: 70% (0.091 g, 0.166 mmol). Recrystallisation from a hot acetonitrile solution gave 1b as green blocks. Anal. Calcd for $C_{28}H_{28}N_4CoCl_2$: C, 61.09; H, 5.09; N, 10.18. Found C, 60.76; H, 5.15; N, 10.12%.

(c) 1c, M = Ni, X = Br. Using an analogous procedure to that described for 1a employing (DME)NiBr$_2$ (0.073 g, 0.238 mmol) and L1 (0.100 g, 0.238 mmol, 1 eq.) gave [{6-{(2,6-i-Pr$_2$C$_6$H$_3$)N=CH}-2,2′:6′,2″-C$_{15}$H$_9$N$_3$}NiBr$_2$] (1c) as an orange solid. Yield: 80% (0.122 g, 0.190 mmol). Anal. Calcd for $C_{28}H_{28}N_4NiBr_2$: C, 52.62; H, 4.39; N, 8.77. Found C, 52.89; H, 4.71; N, 8.64%.

(d) 1d, M = Zn, X = Cl. Using an analogous procedure to that described for 1a employing ZnCl$_2$ (0.032 g, 0.238 mmol) and L1 (0.100 g, 0.238 mmol, 1 eq.) gave [{6-{(2,6-i-Pr$_2$C$_6$H$_3$)N=CH}-2,2′:6′,2″-C$_{15}$H$_9$N$_3$}ZnCl$_2$] (1d) as a pale yellow solid. Yield: 65% (0.086 g, 0.155 mmol). Recrystallisation from an acetonitrile–chloroform solution gave 1d as pale yellow blocks. Anal. Calcd for $C_{28}H_{28}N_4ZnCl_2$: C, 60.39; H, 5.03; N, 10.06. Found C, 60.51; H, 4.99; N, 10.21%.

3.4 Synthesis of [{6-iminoacetyl-2,2′:6′,2″-terpyridine-(2,6- diisopropylanil)}MX$_2$] (2)

(a) 2a, M = Fe, X = Cl. An oven-dried Schlenk flask equipped with a magnetic stir bar was evacuated and back-filled with nitrogen. The flask was charged with anhydrous FeCl$_2$ (0.030 g, 0.238 mmol) in n-BuOH (10 ml) and the contents stirred at 110 °C until the iron salt had completely dissolved. L2 (0.103 g, 0.238 mmol, 1 eq.) was added and the reaction mixture stirred at 110 °C for a further 20 min. After cooling to room temperature, the suspension was concentrated and hexane added to induce precipitation of the product. The solid was filtered off, washed with hexane and dried overnight under reduced pressure to afford [{6-{(2,6-i-Pr$_2$C$_6$H$_3$)N=CMe}-2,2′:6′,2″-C$_{15}$H$_9$N$_3$}FeCl$_2$] (2a) as a dark-purple solid. Yield: 72% (0.096 g, 0.171 mmol). ^{1}H NMR (CDCl$_3$, 293 K): δ 103.4 (<1.6 ms, H$_\alpha$).

(b) 2b, M = Co, X = Cl. Using an analogous procedure to that described for 2a employing anhydrous CoCl$_2$ (0.031 g, 0.238 mmol) and L2 (0.103 g, 0.238 mmol, 1 eq.) gave [{6-{(2,6-i-Pr$_2$C$_6$H$_3$)N=CMe}-2,2′:6′,2″-C$_{15}$H$_9$N$_3$}CoCl$_2$] (2b) as a blue solid. Yield: 70% (0.094 g, 0.166 mmol). ^{1}H NMR (CDCl$_3$, 293 K): δ 95.2 (br, H$_\alpha$).

(c) 2c, M = Ni, X = Br. Using an analogous procedure to that described for 2a employing (DME)NiBr$_2$ (0.073 g, 0.238 mmol) and L2 (0.103 g, 0.238 mmol, 1 eq.) gave [{6-{(2,6-i-Pr$_2$C$_6$H$_3$)N=CMe}-2,2′:6′,2″-C$_{15}$H$_9$N$_3$}NiBr$_2$] (2c) as an orange solid. Yield: 75% (0.117 g, 0.179 mmol). Recrystallisation from a chloroform solution at 0 °C gave 2c as orange plates. ^{1}H NMR (CDCl$_3$, 293 K): δ 130.9 (<0.1 ms, H$_\alpha$), 92.9 (2.07 ms, H$_\beta$H$_{\beta'}$), 82.5 (2.25 ms, H$_\beta$H$_\beta$), 72.3 (2.24 ms, H$_\beta$H$_{\beta'}$), 66.8 (2.54 ms, H$_\beta$H$_{\beta'}$), 59.5 (2.59 ms, H$_\beta$H$_{\beta'}$), 35.0 (3.66 ms, H$_{\beta'\beta'}$), 18.0 (7.37 ms, H$_\gamma$), 16.9 (6.30 ms, H$_\gamma$), 13.3 (8.20 ms, H$_\gamma$), 12.0–4.1 (Ar–H, CMe=N, Ar–CHMe$_2$). Anal. Calcd for $C_{29}H_{30}N_4NiBr_2$: C, 46.69; H, 4.02; N, 7.26. Found C, 47.09; H, 3.97; N, 7.11%.

(d) 2d, M = Zn, X = Cl. Using an analogous procedure to that described for 2a employing anhydrous ZnCl$_2$ (0.032 g, 0.238 mmol) and L2 (0.103 g, 0.238 mmol, 1 eq.) gave [{6-{(2,6-i-Pr$_2$C$_6$H$_3$)N=CMe}-2,2′:6′,2″-C$_{15}$H$_9$N$_3$}ZnCl$_2$] (2d) as a yellow solid. Yield: 65% (0.088 g, 0.155 mmol). Prolonged standing at room temperature of an acetonitrile–chloroform mixture containing the complex gave 2d as pale yellow blocks. Anal. Calcd for $C_{29}H_{30}N_4ZnCl_2$: C, 61.01; H, 5.26; N, 9.82. Found C, 61.21; H, 5.12; N, 9.97%.

3.5 Ethylene oligomerisation

An oven dried 200 ml Schlenk vessel equipped with magnetic stir bar was evacuated and backfilled with nitrogen. The vessel was charged with the precatalyst (0.01 mmol) and dissolved or suspended in toluene (40 ml). MAO (4.0 mmol, 400 eq.) was introduced and the reaction mixture left to stir for 5 minutes. The vessel was purged with ethylene and the contents magnetically stirred under 1 bar ethylene pressure at room temperature for the duration of the test. After 1 h, the test was terminated by the addition of dilute aqueous hydrogen chloride (5 ml). The organic phase was separated and dried over magnesium sulfate and filtered. GC analysis was performed by taking an aliquot of the solution. For analysis of the oligomers by ^{1}H NMR spectroscopy, the solvent was removed on a rotary evaporator and the residue dissolved in CDCl$_3$.

3.6 Density functional calculations

Quantum mechanical calculations have been carried out using the Gaussian 03 package of programs.[23] Density functional theory (DFT) was applied, in particular the functional Becke's three-parameter hybrid exchange method combined with the LYP correlation functional (B3LYP).[24] The quasi-relativistic

Table 8 Crystallographic and data processing parameters for complexes **1a**, **1b**, **1d**, **2c** and **2d**

Complex	1a	1b	1d	2c	2d
Formula	$C_{28}H_{28}Cl_2N_4Fe \cdot CH_3CN$	$C_{28}H_{28}Cl_2N_4Co \cdot CH_3CN$	$C_{28}H_{28}Cl_2N_4Zn \cdot CHCl_3$	$C_{29}H_{30}Br_2N_4Ni \cdot 3.5CHCl_3$	$C_{29}H_{30}Cl_2N_4Zn$
M	588.35	591.43	676.18	1070.89	570.84
Crystal size/mm^3	$0.22 \times 0.17 \times 0.05$	$0.17 \times 0.25 \times 0.35$	$0.20 \times 0.16 \times 0.11$	$0.35 \times 0.23 \times 0.05$	$0.18 \times 0.16 \times 0.13$
T/K	150(2)	150(2)	150(2)	150(2)	150(2)
Crystal system	Monoclinic	Monoclinic	Monoclinic	Monoclinic	Triclinic
Space group	$P2(1)/c$	$P2(1)/c$	$P2(1)/c$	$C2/c$	$P\bar{1}$
a/Å	10.0666(12)	10.089(3)	10.3842(7)	33.824(8)	10.2739(19)
b/Å	17.260(2)	17.124(5)	16.8912(11)	10.759(3)	10.5553(19)
c/Å	16.987(2)	16.991(5)	17.4972(12)	23.446(6)	12.623(2)
α/°	90	90	90	90	94.301(3)
β/°	96.542(2)	96.459(5)	96.1660(10)	100.613(4)	101.922(3)
γ/°	90	90	90	90	96.325(3)
U/Å^3	2932.3(6)	2916.8(15)	3051.3(4)	8386(3)	1324.4(4)
Z	4	4	4	8	2
D_c/Mg m^{-3}	1.333	1.347	1.472	1.696	1.431
$F(000)$	1224	1228	1384	4264	592
μ(Mo-K$_\alpha$)/mm^{-1}	0.724	0.799	1.269	3.068	1.155
Reflections collected	20994	22391	23670	31356	10435
Independent reflections	5155	5730	5986	8219	5134
R_{int}	0.0383	0.0285	0.0366	0.1464	0.0362
Restraints/parameters	0/367	0/407	0/374	0/454	0/330
Final R indices ($I > 2\sigma(I)$)	$R_1 = 0.0408$, $wR_2 = 0.1039$	$R_1 = 0.0336$, $wR_2 = 0.0920$	$R_1 = 0.067$, $wR_2 = 0.0884$	$R_1 = 0.1088$, $wR_2 = 0.2653$	$R_1 = 0.0440$, $wR_2 = 0.1004$
All data	$R_1 = 0.0497$, $wR_2 = 0.1089$	$R_1 = 0.0409$, $wR_2 = 0.0947$	$R_1 = 0.0471$, $wR_2 = 0.0919$	$R_1 = 0.2232$, $wR_2 = 0.3250$	$R_1 = 0.0567$, $wR_2 = 0.1055$
Goodness of fit on F^2 (all data)	1.045	1.036	0.974	0.893	1.003

^{a} Data in common: graphite-monochromated Mo-K$_\alpha$ radiation, $\lambda = 0.710\,73$ Å; $R_1 = \sum\|F_o| - |F_c\|/\sum|F_o|$, $wR_2 = [\sum w(F_o^2 - F_c^2)^2/\sum w(F_o^2)^2]^{1/2}$, $w^{-1} = [\sigma^2(F_o)^2 + (aP)^2]$, $P = [\max(F_o^2,0) + 2(F_c^2)]/3$, where a is a constant adjusted by the program; goodness of fit $= [\sum(F_o^2 - F_c^2)2/(n - p)]^{1/2}$ where n is the number of reflections and p the number of parameters.

effective core potential (ECP) LANL2DZ was used for all metal atoms.[25] The basis set for both atoms in the valence double-ζ contraction was associated with this ECP. The valence double-ζ with polarisation 6-31 G(d) basis was used for N and Cl and the minimal basis STO-3G for C and H.[26,27]

3.7 Crystallography

Data for **1a**, **1b**, **1d**, **2c** and **2d** were collected on a Bruker APEX 2000 CCD diffractometer. Details of data collection, refinement and crystal data are listed in Table 8. The data were corrected for Lorentz and polarisation effects and empirical absorption corrections applied. Structure solution by direct methods or Patterson (**2d**) and structure refinement based on full-matrix least-squares on F^2 employed SHELXTL version 6.10.[28] Hydrogen atoms were included in calculated positions (C–H = 0.96 Å) riding on the bonded atom with isotropic displacement parameters set to 1.5 U_{eq} (C) for methyl H atoms and 1.2 U_{eq} (C) for all other H atoms. All non-H atoms were refined with anisotropic displacement parameters. Atoms C(25) and C(26) in **1b** were disordered and modelled.

CCDC reference numbers 615609–615613.

For crystallographic data in CIF or other electronic format see DOI: 10.1039/b610562a

4 Conclusions

The capacity of Lx to behave as either a tri- or tetra-dentate ligand has been probed through the use of a combined theoretical and synthetic study of a series of 1 : 1 3d metal halide complexes, $[(Lx)MX_2]$ (M = Fe, Co, Ni, Zn). It is apparent that not only the imino-carbon substituent but also the nature of the metal centre influences the bonding mode adopted by Lx. For nickel, both tetra- and tri-dentate bonding modes are possible while for zinc only tridentate bonding is evident. The steric/electronic attributes of the particular imine donor (ketimine vs. aldimine) coupled with stabilisation effects imparted by specific d^n configurations has been offered as an explanation for these trends. Moreover it has been shown that lability of the ketimine donor is most likely to occur for the high spin iron and cobalt complexes although no clear evidence for this has been identified in the complexes prepared. Nevertheless, the propensity for imine coordination has been suggested as an explanation for the very low catalytic activities for ethylene oligomerisation displayed by the iron systems.

Acknowledgements

References

1 (a) C. Piguet, G. Bernardinelli and G. Hopfgartner, *Chem. Rev.*, 1997, **97**, 2005; (b) E. C. Constable, *Adv. Inorg. Chem. Radiochem.*, 1986, **30**, 69.
2 (a) E. C. Constable, Polynuclear Transition Metal Helicates, in *Comprehensive Supramolecular Chemistry*, ed., J. P. Sauvage and M. W. Hosseini, Elsevier, Oxford, 1996, pp. 213–252; (b) J. M. Lehn, J. P. Sauvage, J. Simon, R. Ziessel, C. Piccinni-Leopardi, G. Germain, J. P. Declercq and M. Van Meerssche, *Nouv. J. Chim.*, 1983, **7**, 413; (c) E. C. Constable, M. J. Hannon, P. A. Martin, P.

R. Raithby and D. A. Tocher, *Polyhedron*, 1992, **11**, 2967; (*d*) K. T. Potts, M. Keshavarz-K, F. S. Tham, H. D. Abruna and C. R. Arana, *Inorg. Chem.*, 1993, **32**, 4422.

3 (*a*) D. B. Dell'Amico, F. Calderazzo, M. Curiardi, L. Labella and F. Marchetti, *Inorg. Chem.*, 2004, **43**, 5459 and ref. therein; (*b*) D. B. Dell Amico, F. Calderazzo, U. Englert, L. Labella and F. Marchetti, *J. Chem. Soc., Dalton Trans.*, 2001, 357.

4 (*a*) D. Xiao, Y. Hou, E. Wang, J. Lu, Y. Li, L. Xu and C. Hu, *Inorg. Chem. Commun.*, 2004, **7**, 437; (*b*) W. Henke, S. Kremer and D. Reinen, *Z. Anorg. Allg. Chem.*, 1982, **491**, 124; (*c*) C.-W. Chan, C.-M. Che and S.-M. Peng, *Polyhedron*, 1993, **12**, 2169; (*d*) E. C. Constable, S. M. Elder, J. Healy and D. A. Tocher, *J. Chem. Soc., Dalton Trans.*, 1990, 1669; (*e*) E. C. Constable, S. M. Elder and D. A. Tocher, *Polyhedron*, 1992, **11**, 1337; (*f*) C.-M. Che, C.-W. Chan, S.-M. Yang, C.-X. Guo, C.-Y. Lee and S.-M. Peng, *J. Chem. Soc., Dalton Trans.*, 1995, 2961; (*g*) E. N. Maslen, C. L. Raston and A. H. White, *J. Chem. Soc., Dalton Trans.*, 1975, 323; (*h*) E. C. Constable, M. J. Hannon, P. Harverson, M. Neuburger, D. R. Smith, V. F. Wanner, L. A. Whall and M. Zehnder, *Polyhedron*, 2000, **19**, 23; (*i*) E. C. Constable, S. M. Elder, M. J. Hannon, A. Martin, P. R. Raithby and D. A. Tocher, *J. Chem. Soc., Dalton Trans.*, 1996, 2423.

5 J.-P. Gisselbrecht, M. Gross, J.-M. Lehn, J. P. Sauvage, R. Ziessel, C. Piccinni-Leopardi, J. M. Arrieta, G. Germain and M. van Meerssche, *Nouv. J. Chim.*, 1984, **8**, 661.

6 R. Ziessel, A. Harriman, J. Suffert, M.-T. Youinou, A. De Cian and J. Fischer, *Angew. Chem., Int. Ed. Engl.*, 1997, **36**, 2509.

7 G. J. P. Britovsek, S. P. D. Baugh, O. Hoarau, V. C. Gibson, D. F. Wass, A. J. P. White and D. J. Williams, *Inorg. Chim. Acta*, 2003, **345**, 279.

8 Y. D. M. Champouret, J.-D. Maréchal, I. Dadhiwala, J. Fawcett, D. Palmer and G. A. Solan, *Dalton Trans.*, 2006, 2350.

9 Y. D. M. Champouret, R. K. Chaggar, I. Dadhiwala, J. Fawcett and G. A. Solan, *Tetrahedron*, 2006, **62**, 79.

10 J. Uenishi, T. Tanaka, N. Takakazu, K. Nishiwaki, S. Wakabayashi, S. Oae and H. Tsukube, *J. Org. Chem.*, 1993, **58**, 4382.

11 A. W. Addison, T. N. Rao, J. Reedijk, J. von Rijn and G. C. Verschoor, *J. Chem. Soc., Dalton Trans.*, 1984, 1349.

12 M. J. Al-Khatib, J. Fawcett and G. A. Solan, unpublished results.

13 E. Szajna, P. Dobrowolski, A. L. Fuller, A. M. Arif and L. M. Berreau, *Inorg. Chem.*, 2004, **43**, 3988.

14 For use of the ν(CO) stretch as a guide to relative donor capability of imines/pyridines see: (*a*) M. Brockmann, H. tom Dieck and J. Klaus, *J. Organomet. Chem.*, 1986, **301**, 209; (*b*) S. Morton and J. F. Nixon, *J. Organomet. Chem.*, 1985, **282**, 123; (*c*) L. Gonsalvi, J. A. Gaunt, H. Adams, A. Castro, G. J. Sunley and A. Haynes, *Organometallics*, 2003, **22**, 1047.

15 (*a*) A. R. Rossi and R. Hoffmann, *Inorg. Chem.*, 1975, **2**, 365; (*b*) S. Alvarez and J. Ciera, *Angew. Chem., Int. Ed.*, 2006, **45**, 3012.

16 For reviews see: (*a*) V. C. Gibson and S. K. Spitzmesser, *Chem. Rev.*, 2003, **103**, 283; (*b*) G. J. P. Britovsek, V. C. Gibson and D. F. Wass, *Angew. Chem., Int. Ed.*, 1999, **38**, 428; (*c*) S. D. Ittel, L. K. Johnson and M. Brookhart, *Chem. Rev.*, 2000, **100**, 1169; (*d*) S. Mecking, *Angew. Chem., Int. Ed.*, 2001, **40**, 534.

17 (*a*) P. J. Flory, *J. Am. Chem. Soc.*, 1940, **62**, 1561; (*b*) G. V. Schulz, *J. Phys. Chem. B*, 1939, **43**, 25.

18 Y. Nakayama, Y. Baba, H. Yasuda, K. Kawakita and N. Ueyama, *Macromolecules*, 2003, **36**, 7953.

19 W. L. F. Armarego and D. D. Perrin, *Purification of Laboratory Chemicals*, Butterworth Heinemann, London, 4th edn, 1996.

20 F. E. Mabbs and D. J. Machin, *Magnetism and Transition Metal Complexes*, Chapman and Hall, London, 1973.

21 (*a*) C. J. O'Connor, *Prog. Inorg. Chem.*, 1982, **29**, 203; (*b*) *Handbook of Chemistry and Physics*, ed. R. C. Weast, CRC Press, Boca Raton, FL, 70th edn, 1990, p. E134.

22 G. R. Newkome, D. C. Hager and G. E. Kiefer, *J. Org. Chem.*, 1986, **51**, 850.

23 M. J. Frisch, G. W. Trucks, H. B. Schlegel, G. E. Scuseria, M. A. Robb, J. R. Cheeseman, J. A. Montgomery, Jr, T. Vreven, K. N. Kudin, J. C. Burant, J. M. Millam, S. S. Iyengar, J. Tomasi, V. Barone, B. Mennucci, M. Cossi, G. Scalmani, N. Rega, G. A. Petersson, H. Nakatsuji, M. Hada, M. Ehara, K. Toyota, R. Fukuda, J. Hasegawa, M. Ishida, T. Nakajima, Y. Honda, O. Kitao, H. Nakai, M. Klene, X. Li, J. E. Knox, H. P. Hratchian, J. B. Cross, V. Bakken, C. Adamo, J. Jaramillo, R. Gomperts, R. E. Stratmann, O. Yazyev, A. J. Austin, R. Cammi, C. Pomelli, J. W. Ochterski, P. Y. Ayala, K. Morokuma, G. A. Voth, P. Salvador, J. J. Dannenberg, V. G. Zakrzewski, S. Dapprich, A. D. Daniels, M. C. Strain, O. Farkas, D. K. Malick, A. D. Rabuck, K. Raghavachari, J. B. Foresman, J. V. Ortiz, Q. Cui, A. G. Baboul, S. Clifford, J. Cioslowski, B. B. Stefanov, G. Liu, A. Liashenko, P. Piskorz, I. Komaromi, R. L. Martin, D. J. Fox, T. Keith, M. A. Al-Laham, C. Y. Peng, A. Nanayakkara, M. Challacombe, P. M. W. Gill, B. Johnson, W. Chen, M. W. Wong, C. Gonzalez and J. A. Pople, *GAUSSIAN 03*, Gaussian Inc., Wallingford, CT, 2004.

24 (*a*) A. D. Becke, *J. Chem. Phys.*, 1993, **98**, 5648; (*b*) C. Lee, W. Yang and R. G. Parr, *Phys. Rev. B: Condens. Matter*, 1988, **37**, 785; (*c*) P. J. Stephens, F. J. Devlin, C. F. Chabalowski and M. J. Frisch, *J. Phys. Chem.*, 1994, **98**, 11623.

25 P. J. Hay and W. R. Wadt, *J. Chem. Phys.*, 1985, **82**, 299.

26 W. J. Hehre, R. Ditchfield and J. A. Pople, *J. Chem. Phys.*, 1972, **56**, 2257.

27 P. C. Hariharan and J. A. Pople, *Theor. Chim. Acta*, 1973, **28**, 213.

28 G. M. Sheldrick, *SHELXTL Version 6.10*, Bruker AXS Inc., Madison, Wisconsin, USA, 2000.